JACS
JOURNAL OF THE AMERICAN CHEMICAL SOCIETY
pubs.acs.org/JACS
Article

Symmetry-Guided Synthesis of *N,N′*-Bicarbazole and Porphyrin-Based Mixed-Ligand Metal–Organic Frameworks: Light Harvesting and Energy Transfer

Christian Fiankor, James Nyakuchena, Rebecca Shu Hui Khoo, Xu Zhang, Yuchen Hu, Sizhuo Yang, Jier Huang,* and Jian Zhang*

Cite This: https://doi.org/10.1021/jacs.1c10291
Read Online

ABSTRACT: In the past decades, many attempts have been made to mimic the energy transfer (EnT) in photosynthesis, a key process occurring in nature that is of fundamental significance in solar fuels and sustainable energy. Metal–organic frameworks (MOFs), an emerging class of porous crystalline materials self-assembled from organic linkers and metal or metal cluster nodes, offer an ideal platform for the exploration of directional EnT phenomena. However, placing energy donor and acceptor moieties within the same framework with an atomistic precision appears to be a major synthesis challenge. In this work, we report the design and synthesis of a highly porous and photoactive *N,N′*-bicarbazole- and porphyrin-based mixed-ligand MOF, namely, NPF-500-H_2TCPP (NPF = Nebraska porous framework; H_2TCPP = *meso*-tetrakis(4-carboxyphenyl)porphyrin), where the secondary ligand H_2TCPP is incorporated precisely through the open metal sites of the equatorial plane of the octahedron cage resulting from the underlying (4,8) connected network of NPF-500. The efficient EnT process from *N,N′*-bicarbazole to porphyrin in NPF-500-H_2TCPP was captured by time-resolved spectroscopy and exemplified by photocatalytic oxidation of thioanisole. These results demonstrate not only the capability of NPF-500 as the scaffold to precisely arrange the donor–acceptor assembly for the EnT process but also the potential to directly utilize the EnT process for photocatalytic applications.

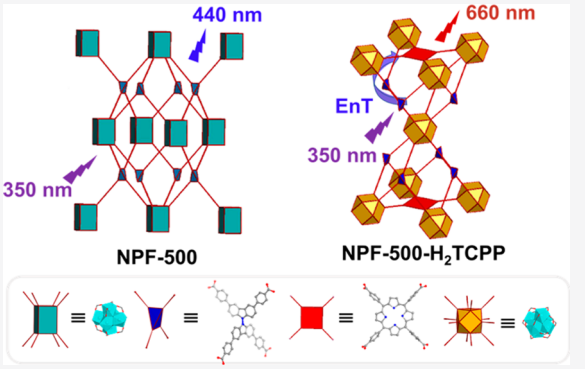

INTRODUCTION

As one of the essential processes in nature, photosynthesis relies on the efficient excited state energy transfer (EnT) between chlorophyll and carotenoid networks present in flora to harvest solar energy and transport it to the reaction center with over 95% efficiency.[1] Many efforts have been devoted to design highly efficient EnT systems that mimic photosynthesis, including covalently bonded porphyrin arrays,[2] dendrimers,[3] polymers,[4] and donor–acceptor supramolecular systems, among others.[5] To achieve fast and efficient EnT, it is important to have an optimal distance, alignment, orientation, and precise energy matching, i.e., a large spectral overlap of donor's emission and acceptor's absorption.[6] Since the typical EnT process is most effective through the assembly of an ordered network, metal–organic frameworks[7] (MOFs), a class of crystalline porous hybrid materials constructed from the self-assembly of organic linkers and secondary building units (SBUs), provide an ideal platform to construct photosynthesis mimics.[8−14] Indeed, the crystalline periodicity, molecular-scale porosity, and broad structural, topological, and compositional tunability[15] of MOFs facilitate multistep hopping of the excited state in the network, leading to phenomena ranging from amplified quenching to light-harvesting,[16] as well as transporting remotely collected energy to sites proximal to an energy-converting catalyst, redox shuttle, or electrode.[17,18] As such, these porous framework materials have been widely studied for photocatalysis and fluorescence sensing where EnT plays an important role.[19−23]

Although building photoactive MOFs using a single type of chromogenic linker is straightforward, synthesizing mixed-ligand MOFs using both energy donors and acceptors, especially with an atomistic precision, requires special design and synthesis. To date, arguably the most commonly used strategy for the synthesis of light-harvesting mixed-ligand MOFs involves paddlewheel-type, photoactive 2-D metal–organic layers based on divalent Zn^{2+}, pillared by a second

Received: September 28, 2021

photoactive linker.[24−31] Synthesizing high-valent metal (e.g., Zr^{4+}, Ti^{4+}, Al^{3+}, etc.) containing MOFs that can further increase chemical stabilities of EnT mimics is desirable yet challenging since the robust metal−ligand bonds in these systems typically limit the coordinative reversibility needed to form ordered crystalline structures. Several recent works have opted for Zr-based MOFs to build EnT systems with increased chemical stability;[32−38] however the precise placement of donor and acceptor in geometrically distinct positions with atomistic precision is extremely challenging to be realized. One example was just reported by Li and co-workers[39] involving a stepwise linker insertion strategy[40] to install the energy acceptor into a framework composed of an energy donor ligand (and vice versa).

Herein, we report the symmetry-guided, one-pot synthesis of mixed-ligand MOFs for light harvesting and EnT using two topologically distinct linkers. Our design is based on a highly porous and photoactive *N,N′*-bicarbazole-based Zr-MOF with a **flu** topology, namely, NPF-500 (NPF = Nebraska porous framework). The octahedral cage of NPF-500 has a square-shaped pocket that, with the symmetry and size-matching, enables the coordination of secondary porphyrin-based ligands: H_2TCPP and NiTCPP (TCPP = *meso*-tetrakis(4-carboxyphenyl)porphyrin). Using a one-pot synthesis, we were able to construct mixed-ligand MOFs, i.e., NPF-500-H_2TCPP and NPF-500-NiTCPP, with a **pfm** topology. The strong spectral overlap between the emission spectrum of *N,N′*-bicarbazole (as the energy donor) and absorption spectrum of porphyrin (as the energy acceptor) enables NPF-500-H_2TCPP as an efficient EnT system, which is exemplified by time-resolved fluorescence spectroscopy and utilized to enhance the photocatalytic efficiency of oxygenation of thioanisole.

RESULTS AND DISCUSSION

Structural Design. The assembly of mixed-ligand MOFs with complex and well-ordered pore architectures can be achieved by a series of topologically distinct linkers bearing various functional groups;[41−45] however, for high-valent metal containing MOFs such as Zr-MOFs, more rational design is usually required to obtain an ordered structure.[46] Our design stems from the recognition of the 4-fold symmetry of the commercially available tetratopic square-planar ligand, H_2TCPP, which is also a common energy acceptor used in constructing EnT mimics. In order to incorporate H_2TCPP into a host framework that consists of empty pockets with matching size and symmetry, we surveyed Zr-MOFs reported to date with inherent, coordinately unsaturated metal sites and identified PCN-521, a (4,8) network composed of a tetrahedral ligand $H_4\mathbf{L_0}$ with a tetraphenylmethane core (Scheme 1) and 8-connected Zr_6 cluster with a **flu** topology.[47] The octahedral cage in PCN-521 contains a square-shaped pocket along the equatorial plane, which well matches the size of H_2TCPP: the O−O distance of 20.2 Å between the two diagonal pairs of terminal $H_2O/-OH^-$ groups along the *ab* plane in PCN-521 is close to the O−O distance between the two *trans*-carboxyls in H_2TCPP (~19.7 Å) (see Supporting Information, Figure S8).

Scheme 1. Chemical Structures of Tetraphenylmethane, $H_4\mathbf{L_0}$, and *N,N′*-Bicarbazole

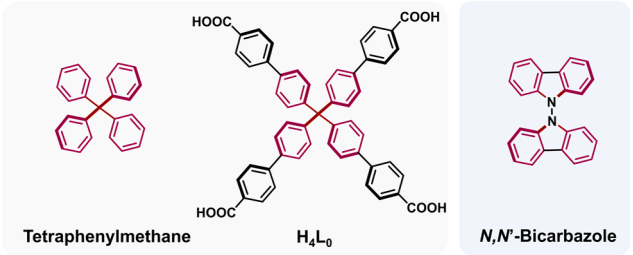

An interesting structural analogue of tetraphenylmethane is *N,N′*-bicarbazole (Scheme 1), of which the two carbazole planes often adopt a pseudoperpendicular geometry and thus a similar S_4 symmetry to tetraphenylmethane.[48−51] More importantly, derivatives of *N,N′*-bicarbazole often exhibit emission peaks close to 450 nm,[52−54] which well overlap with the absorption band of H_2TCPP. Therefore, we designed a new tetratopic ligand $H_4\mathbf{L}$ (Figure 1a) based on *N,N′*-bicarbazole for two reasons: (1) its tetrahedral geometry and similar size to ligand $H_4\mathbf{L_0}$ likely result in the formation of a Zr-MOF with the same (4,8)-connected **flu** net as PCN-521, which consists similar empty pockets matching the size of H_2TCPP; (2) it is likely to emit in a suitable wavelength window and serve as a good donor to transfer energy to H_2TCPP.

MOF Synthesis and Structural Description. *N,N′*-Bicarbazole-based tetratopic ligand $H_4\mathbf{L}$ was synthesized via an oxidative coupling of 3,6-dibromocarbazole and subsequent Suzuki coupling, followed by hydrolysis in a basic medium (see Supporting Information S-1 for the detailed synthesis procedure). Colorless truncated octahedron-shaped crystals of NPF-500 were obtained by a solvothermal reaction of $ZrOCl_2{\cdot}8H_2O$ and $H_4\mathbf{L}$ in the presence of benzoic and trifluoroacetic acid acting as co-modulating agents at 120 °C for 24 h. Single-crystal X-ray diffraction studies at 273 K reveal that NPF-500 crystallizes in space group *I4/mmm* (no. 139, Table S4) of the tetragonal system with the lattice parameters $a = b = 20.406$ Å, $c = 43.613$ Å. Consistent with our prediction, NPF-500 is indeed a noninterpenetrated (4,8)-net where each tetrahedral ligand connects to four Zr_6 clusters in a 2:1 ratio and exhibits the **flu** topology with a charge-balanced framework formula of $Zr_6O_4(OH)_8(H_2O)_4\mathbf{L}_2$. Each Zr_6 cluster is coordinated by eight carboxylate groups from eight **L** ligands, with four above and four below the equatorial plane, while the remaining sites are capped with four pairs of terminal $H_2O/-OH^-$ groups. Powder X-ray diffraction (PXRD) patterns of NPF-500 confirm the bulk phase purity of the as-synthesized sample when compared to the simulated patterns from its corresponding single-crystal structure (Figure S11).

The successful formation of the **flu** net in NPF-500 is likely because *N,N′*-bicarbazole exhibits a similar geometric deviation from the ideal tetrahedron to that observed for ligand $H_4\mathbf{L_0}$ in PCN-521 (Figure S10). The interstitial octahedral cage in NPF-500 has a size of 20.9 Å × 20.9 Å × 36.4 Å, and its square equilateral plane matches well with H_2TCPP. However, our initial attempts using solvent-assistant ligand incorporation (SALI)[55] to integrate H_2TCPP into presynthesized NPF-500 proved unsuccessful. This result is likely due to the retarded diffusion of the relatively large H_2TCPP molecule through the small open windows (12.4 Å × 12.6 Å) of NPF-500. We next employed a one-pot synthesis and utilized both primary ligand $H_4\mathbf{L}$ and secondary ligand H_2TCPP to construct mixed-ligand MOFs. Briefly, solvothermal reaction of $ZrCl_4$, $H_4\mathbf{L}$, and H_2TCPP in the presence of benzoic and acetic acid acting as co-modulating agents in DMF at 110 °C for 12 h. To our delight, purple truncated octahedral crystals of NPF-500-

https://doi.org/10.1021/jacs.1c10291
J. Am. Chem. Soc. XXXX, XXX, XXX−XXX

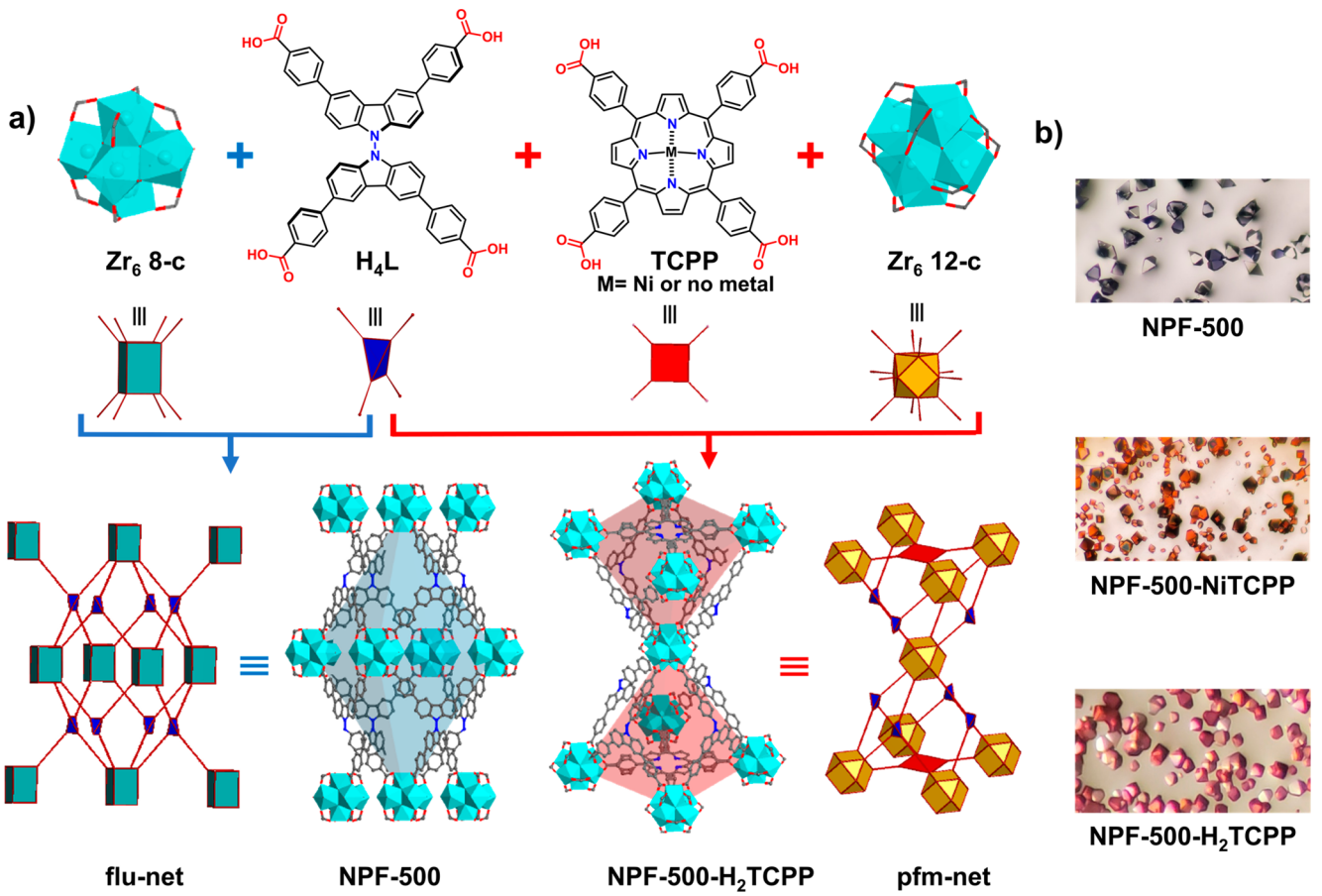

Figure 1. (a) Chemical structures of Zr_6 clusters, H_4**L**, and H_2TCPP/NiTCPP and the formation of NPF-500, NPF-500-H_2TCPP/NiTCPP, and their topological representations (C, gray; O, red; N, blue; Zr, cyan polyhedra). (b) Photographs of single crystals of NPF-500, NPF-500-NiTCPP, and NPF-500-H_2TCPP.

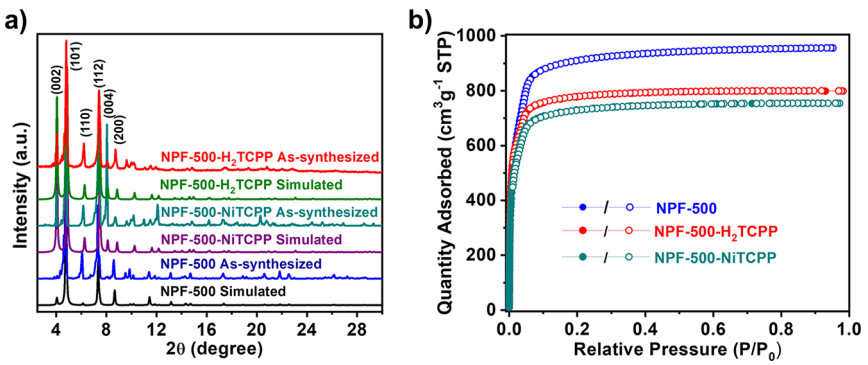

Figure 2. (a) Powder X-ray diffraction patterns and (b) N_2 sorption isotherms of NPF-500, NPF-500-H_2TCPP, and NPF-500-NiTCPP.

H_2TCPP were obtained (Figure 1b and Figure S5) after screening the reaction conditions including the metal/ligand ratio, modulator, etc. (Table S2). Similarly, replacement of H_2TCPP by NiTCPP in the synthesis results in orange truncated octahedral crystals of NPF-500-NiTCPP that are suitable for single-crystal X-ray diffraction (Figure 1b and Figure S5).

Single-crystal X-ray diffraction reveals that NPF-500-NiTCPP crystallizes in space group $I\bar{4}$ (No. 82, Table S6) of the tetragonal system in a cell of dimensions $a = b = 19.952$ Å, $c = 43.590$ Å. The structure of NPF-500-NiTCPP involves the assembly of a 12-connected Zr_6 cluster, 4-connected ligand **L**, and 4-connected NiTCPP. Each Zr_6 cluster is coordinated with eight carboxylates from **L**, four above and four below the equatorial plane, like that observed in NPF-500. A remarkable difference is that the equatorial plane of the Zr_6 cluster in NPF-500-NiTCPP is bridged by four carboxylates from four NiTCPP ligands resulting in an extended (4,4,12)-connected network with the formula $Zr_6O_4(OH)_4L_2$(NiTCPP). Overall, NPF-500-NiTCPP is a trinodal net exhibiting the **pfm** topology with the point symbol $(4^{32}.6^{30}.8^4)(4^4.6^2)(4^6)_2$ calculated using the TOPOS program.[56] It should be noted that this is the first time two tetracarboxylate ligands of distinct symmetry (i.e., tetrahedral and square planar) are assembled into a mixed-ligand Zr-MOF via one-pot synthesis. NPF-500-H_2TCPP also crystallizes in space group $I\bar{4}$ and is an

https://doi.org/10.1021/jacs.1c10291
J. Am. Chem. Soc. XXXX, XXX, XXX−XXX

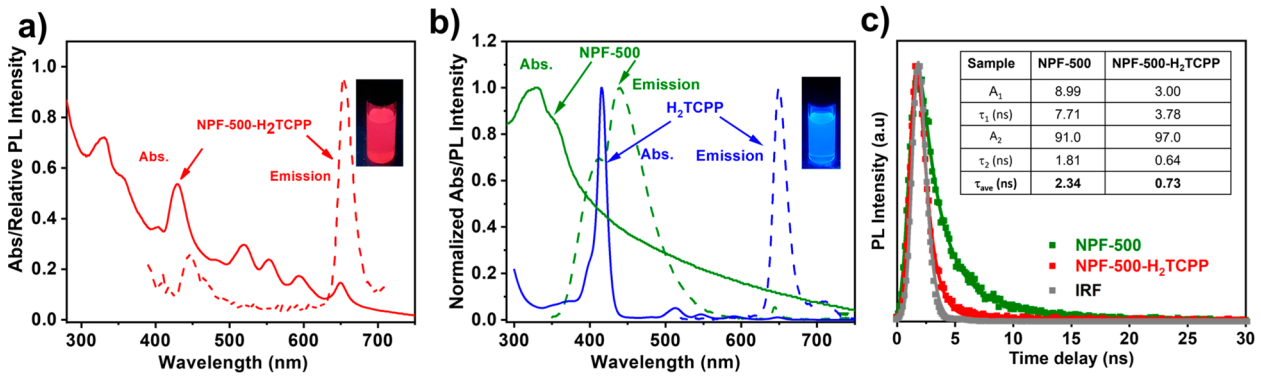

Figure 3. (a) UV−vis absorption and emission (λ_{ex} = 350 nm) spectra of NPF-500-H_2TCPP. Inset is the photograph of NPF-500-H_2TCPP under UV light irradiation. (b) UV−vis absorption and emission (λ_{ex} = 350 nm) spectra of NPF-500 and H_2TCPP. Inset is the photograph of NPF-500 under UV light irradiation. (c) Emission lifetime decay at 440 nm of NPF-500 and NPF-500-H_2TCPP following 280 nm excitation.

isostructure of NPF-500-NiTCPP, and the PXRD patterns of both frameworks confirm the bulk phase purity (Figure 2a).

One structural feature of both mixed-ligand MOFs is their lowered symmetry compared to the parent framework NPF-500. In mixed-ligand MOFs, Zr_6 clusters deviate from the original orientations along the *ab* plane, and the carboxylate groups of the TCPP linker thus adopt a monodentate coordination mode (η^1) via one O atom (Figure S9). This is in contrast to the common dinuclear-bridged, bidentate coordination mode (μ-η^1,η^1) of the carboxylate ligand in typical Zr-MOFs such as UiO-66. Since the distance between the two diagonal pairs of terminal H_2O/$-OH^-$ groups in original NPF-500 of 20.9 Å is slightly longer than the dimension of TCPP (19.7 Å), such change can facilitate the monodentate coordination mode for a better size matching (Figure S9). To our delight, the change to monodentate coordination mode does not compromise the chemical stability of the mixed-ligand MOFs (*vide infra*).

Stability and Porosity. The thermal stability of three NPF-500 series MOFs was assessed by thermogravimetric analysis (TGA) under N_2 (Figures S29, Supporting Information). The initial weight loss before 150 °C is attributed to the removal of the solvent molecules in the pores. It is interesting to note the weight loss from 200 to 350 °C that can be attributed to the removal of strongly coordinated modulating agents in NPF-500 is absent in both mixed-ligand MOFs. This is consistent with the removal of the modulators by the occupancy of a porphyrin linker at the uncoordinated sites of the Zr_6 cluster in the mixed-ligand MOFs. All NPF-500 series Zr-based MOFs exhibit a significant thermal decomposition around 540 °C, pointing to their excellent thermal stability. In addition, the chemical stability of the NPF-500 series was examined by treating MOFs in H_2O, basic (pH = 11), and acidic (pH = 1) conditions, and excellent crystallinity remains after 24 h based on the PXRD patterns (Figures S12−S16 and Figures S19−S21).

After activation using supercritical CO_2 exchange, the permanent porosity of the NPF-500 series was confirmed by N_2 adsorption isotherms measured at 77 K (Figure 2b). NPF-500 exhibits a typical type I isotherm, with a saturated N_2 uptake of 956 cm^3 g^{-1}, a Brunauer−Emmett−Teller surface area (SA_{BET}) of 3737 m^2g^{-1}, and a pore volume of 1.48 cm^3 g^{-1}. After the incorporation of the porphyrin ligand, a slightly decreased SA_{BET} of 2929 and 3107 m^2 g^{-1} for NPF-500-NiTCPP and NPF-500-H_2TCPP, respectively, resulted. The solvent-accessible volume calculated by PLATON for NPF-500 is 81.8%, while that of NPF-500-NiTCPP and NPF-500-H_2TCPP is 71.3% and 70.9%, respectively.

Control of Linker Ratio. Mixed-ligand MOFs that are composed of ligands with the same length and symmetry usually form as a single phase with variable linker ratios.[57−59] However, the tetrahedral bicarbazole ligand **L** and square-planar TCPP in NPF-500-NiTCPP are geometrically distinct. Thus, the linker ratios that can be realized within NPF-500-NiTCPP should be studied in detail. In our investigation, the concentration of the modulating reagent (i.e., benzoic acid) and H_4**L** ligand was kept constant, while the concentration of NiTCPP was systematically increased. PXRD was used to identify the presence of product with different structure. As shown in Figure 2a, the PXRD patterns of NPF-500 and NPF-500-NiTCPP are similar since the incorporation of the NiTCPP into the NPF-500 framework does not significantly change the unit cell, and they are considered as the same phase. To our delight, the phase purity has a large tolerance on the linker ratio; that is, as the amount of NiTCPP increases, NPF-500-NiTCPP starts to form as a pure phase exemplified by the uniform shape and color of the single crystals (Figure S17). Formation of MOFs that are solely based on NiTCPP such as PCN-222[60] or PCN-224[61] was not observed in our study, as confirmed by PXRD (Figure S18). Eventually a high NiTCPP:H_4**L** ratio close to the ideal value of 0.5 (100% occupancy) can be obtained without the formation of any impurity (Figure S6). A similar degree of controlling the linker ratio was observed in NPF-500-H_2TCPP (*vide infra*).

Fluorescence Measurement. The formation of NPF-500-H_2TCPP was further confirmed by UV−visible absorption spectroscopy. As shown in Figure 3a, the spectrum of NPF-500-H_2TCPP exhibits an absorption band at 350 nm that can be attributed to ligand **L** in NPF-500 and several characteristic bands from 420 to 650 nm that are originated from H_2TCPP (Figure 3b), supporting the presence of both ligands in the MOF. Following the excitation at 350 nm, the emission spectrum of NPF-500 exhibits a broad band centered at ∼440 nm (Figure 3b), which is consistent with the emission band of H_4**L** (Figure S34) and can thus be attributed to the emission of H_4**L** in NPF-500. On the other hand, H_2TCPP has an emission band at 660 nm following the excitation at 425 nm (Figure 3b). The significant spectral overlap between the emission spectrum of **L** in NPF-500 and the absorption spectrum of H_2TCPP, in combination with the close distance between the two linkers in NPF-500-H_2TCPP (14.8 Å), strongly suggests the feasibility of the construction of an efficient Förster-type

https://doi.org/10.1021/jacs.1c10291
J. Am. Chem. Soc. XXXX, XXX, XXX−XXX

resonant energy transfer (FRET) system where H_4**L** and H_2TCPP are the energy donor and acceptor, respectively.[6] Indeed, the emission spectrum of NPF-500-H_2TCPP (Figure 3a) following the selective excitation of H_4**L** in NPF-500-H_2TCPP shows a prominent emission band at 660 nm that results from the emission of H_2TCPP, which unambiguously confirms that EnT occurs from **L** in NPF-500 to H_2TCPP. The presence of some residue emission from **L** suggests that the EnT is not complete. Nevertheless, the quenching does not occur in the physical mixture of H_4**L** and H_2TCPP (Figure S35) and is also not observed in the mixture of NPF-500 and H_2TCPP (Figure S36), underlining the importance of the close distance and/or orientation between the partners of this EnT process. Time-resolved emission experiments based on the time-correlated single-photon counting (TCSPC) technique was employed to further confirm the presence of the EnT process in NPF-500-H_2TCPP. As shown in Figure 3c, compared to the emission lifetime of **L** in NPF-500 collected at 440 nm, the emission lifetime of **L** in NPF-500-H_2TCPP is significantly shortened following the excitation at 280 nm, suggesting that the presence of H_2TCPP quenches **L** emission, which is consistent with the EnT process assigned above. The emission decay kinetics of **L** in both NPF-500 and NPF-500-H_2TCPP can be fit by a multiexponential decay function. The average emission lifetime obtained from the best fitting (Figure 3c) is 2.34 and 0.73 ns for NPF-500 and NPF-500-H_2TCPP, respectively. According to these emission lifetimes, the EnT time and efficiency can be estimated using the following equations:[16,62]

$$1/\tau_{\text{NPF-500-H2TCPP}} = 1/\tau_{\text{NPF-500}} + 1/\tau_{\text{EnT}} \quad (1)$$

$$\eta = 1/\tau_{\text{EnT}}/(1/\tau_{\text{NPF-500}} + 1/\tau_{\text{EnT}}) \quad (2)$$

where $\tau_{\text{NPF-500-H2TCPP}}$ and $\tau_{\text{NPF-500}}$ are the emission decay times for NPF-500-H_2TCPP and NPF-500, respectively, and τ_{EnT} is the EnT time. The obtained EnT rate and efficiency are 0.94 ns^{-1} and 69%, respectively. Note that the orientation of the dipole moment of the donor and acceptor in NPF-500-H_2TCPP with a fixed spatial arrangement might prevent a higher EnT efficiency.[21] Nevertheless, this EnT efficiency is comparable to many previously reported EnT systems based on mixed-ligand or porphyrin-based MOFs,[10,37,63,64] which not only suggests the great potential of our mixed-ligand MOFs as efficient light-harvesting materials for photocatalytic applications but also demonstrates the capability of the symmetry-guided approach for constructing functional mixed-ligand MOFs.

Having established the efficient EnT in NPF-500-H_2TCPP, we next turn to the demonstration of the potential use of such a process to enhance the photocatalytic activity of the mixed-ligand MOF. Here, photosensitized oxygenation of thioanisole was chosen, and the reaction was studied in the presence of oxygen and NPF-500-H_2TCPP (0.2 mol % based on H_2TCPP) under irradiation with a CFL (compact fluorescent lamp, 26 W) (see the Supporting Information for detailed procedure). The donor-only NPF-500 exhibits no activity for this reaction, while NPF-500-H_2TCPP was able to selectively oxidize thioanisole to the corresponding sulfoxide in 99% yield within 1 h (Table 1, entries 1, 2). No apparent overoxidation product of sulfone was observed, consistent with the expected singlet oxygen promoted oxidation mechanism. Control experiments revealed the essential role of light, photocatalyst, and O_2 in this reaction (Table S8). Although H_2TCPP can also promote this reaction in a similar efficiency (Table 1, entry 3), it cannot be easily recycled. On the contrary, NPF-500-H_2TCPP can be repeatedly used for five times without significant decrease of the activity (Table 1, entry 4) and can also exhibit excellent stability indicated by its well-preserved crystalline nature after reaction (Figure S39).To our surprise, PCN-222, a Zr-MOF solely based on H_2TCPP, only shows a moderate oxidation efficiency of 41% (Table 1, entry 5). This likely results from the self-quenching effect due to the close distance between the chromophores in the framework as supported by the prominently reduced emission lifetime of PCN-222 compared with that of H_2TCPP (Figure S37).

Table 1. Photosensitized Oxygenation of Thioanisole

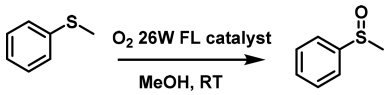

entry	photocatalyst	catalyst loading (%)	conversion (%)
1	NPF-500	0	0
2	NPF-500-H_2TCPP	0.2	99
3	H_2TCPP	0.2	99
4	NPF-500-H_2TCPP	0.2	97[a]
5	PCN-222	0.2	41

[a]Recycled for five times.

To demonstrate the application of EnT in NPF-500-H_2TPP for photocatalysis, we synthesized a series of mixed-ligand MOFs with different **L**:H_2TCPP ratios. Four samples, namely, NPF-500-H_2TCPP-A,B,C,D, were synthesized, and the occupancy percentage of H_2TCPP was determined by ^{1}H NMR spectroscopy after base digestion as 68%, 40%, 16%, and 9%, respectively. When the amount of H_2TCPP in the mixed-ligand MOFs was kept constant, NPF-500-H_2TCPP-C (16% H_2TCPP) exhibits the highest photocatalytic activity (73% conversion in 20 min, Table S9, entry 3), which strongly suggests the effectiveness of EnT in enhancing its photocatalytic activity. Another comparison of these four mixed-ligand MOFs was conducted where the amount of energy donor **L** was kept constant. NPF-500-H_2TCPP-C again gave a higher conversion (65% conversion in 20 min) than NPF-500-H_2TCPP-A (51% conversion), despite a significant lower content of H_2TCPP (16% vs 68%) (Table S9, entries 5 and 6). These results provide solid proof that with an optimal D:A ratio the EnT process indeed can be utilized for enhanced efficiency in photocatalysis.

CONCLUSION

In summary, using symmetry-guided synthesis we have successfully constructed mixed-ligand MOFs using two geometrically distinct tetrahedral *N,N′*-bicarbazole and square-planar porphyrin-based ligands. The close match of the size and shape between the equatorial plane of the octahedron cage in NPF-500 and photoactive porphyrin ligand H_2TCPP results in the ideal assembly of a donor−acceptor construct for light harvesting and energy transfer. The spatial closeness combined with the strong spectral overlap between the emission of the *N,N′*-bicarbazole-based donor and TCPP acceptor facilitates an efficient energy transfer event, which is confirmed by fluorescence spectroscopy. We further demonstrate the utility of the EnT principle in designing efficient photocatalysts using a photosensitized thioanisole oxidation reaction. In view of the versatile photochemical properties of

https://doi.org/10.1021/jacs.1c10291
J. Am. Chem. Soc. XXXX, XXX, XXX−XXX

porphyrin, this work provides a blueprint for the future design of new efficient light-harvesting and novel photocatalytic systems.

■ ASSOCIATED CONTENT

Supporting Information

The Supporting Information is available free of charge at https://pubs.acs.org/doi/10.1021/jacs.1c10291.

Synthesis, experimental data and procedures, X-ray diffraction, UV−vis absorption, and photoluminescence data (PDF)

Accession Codes

CCDC 2103173−2103175 contain the supplementary crystallographic data for this paper. These data can be obtained free of charge via www.ccdc.cam.ac.uk/data_request/cif, or by emailing data_request@ccdc.cam.ac.uk, or by contacting The Cambridge Crystallographic Data Centre, 12 Union Road, Cambridge CB2 1EZ, UK; fax: +44 1223 336033.

■ AUTHOR INFORMATION

Corresponding Authors

Jier Huang − *Department of Chemistry, Marquette University, Milwaukee, Wisconsin 53201, United States;* orcid.org/0000-0002-2885-5786; Email: jier.huang@marquette.edu

Jian Zhang − *Department of Chemistry, University of Nebraska−Lincoln, Lincoln, Nebraska 68588, United States; The Molecular Foundry, Lawrence Berkeley National Laboratory, Berkeley, California 94720, United States;* orcid.org/0000-0003-0274-0814; Email: jianzhang@lbl.gov, jzhang3@unl.edu

Authors

Christian Fiankor − *Department of Chemistry, University of Nebraska−Lincoln, Lincoln, Nebraska 68588, United States*

James Nyakuchena − *Department of Chemistry, Marquette University, Milwaukee, Wisconsin 53201, United States*

Rebecca Shu Hui Khoo − *The Molecular Foundry, Lawrence Berkeley National Laboratory, Berkeley, California 94720, United States*

Xu Zhang − *Jiangsu Engineering Laboratory for Environmental Functional Materials, School of Chemistry and Chemical Engineering, Huaiyin Normal University, Huaian, Jiangsu 223300, China*

Yuchen Hu − *Department of Chemistry, University of Nebraska−Lincoln, Lincoln, Nebraska 68588, United States*

Sizhuo Yang − *Department of Chemistry, Marquette University, Milwaukee, Wisconsin 53201, United States*

Complete contact information is available at: https://pubs.acs.org/10.1021/jacs.1c10291

Notes

The authors declare no competing financial interest.

■ ACKNOWLEDGMENTS

J.Z. thanks NSF/CBET-1706632 for the support of this research. J.N. and J.H. acknowledge the support from NSF/CBET-1706971. Chem-MatCARS Sector 15 is principally supported by the Divisions of Chemistry (CHE) and Materials Research (DMR), National Science Foundation, under grant number NSF/CHE-1346572. Use of the APS, an Office of Science User Facility operated for the U.S. DOE Office of Science by ANL, was supported under Contract No. DE-AC02-06CH11357. Work at the Molecular Foundry and Advanced Light Source was supported by the Office of Science, Office of Basic Energy Sciences, of the U.S. Department of Energy under Contract No. DE-AC02-05CH11231.

■ REFERENCES

(1) Scholes, G. D.; Fleming, G. R.; Olaya-Castro, A.; van Grondelle, R. Lessons from nature about solar light harvesting. *Nat. Chem.* **2011**, *3* (10), 763−774.

(2) Tanaka, T.; Osuka, A. Conjugated porphyrin arrays: synthesis, properties and applications for functional materials. *Chem. Soc. Rev.* **2015**, *44* (4), 943−969.

(3) Li, W. S.; Aida, T. Dendrimer porphyrins and phthalocyanines. *Chem. Rev.* **2009**, *109* (11), 6047−6076.

(4) Jiang, Y.; McNeill, J. Light-Harvesting and Amplified Energy Transfer in Conjugated Polymer Nanoparticles. *Chem. Rev.* **2017**, *117* (2), 838−859.

(5) Wasielewski, M. R. Self-assembly strategies for integrating light harvesting and charge separation in artificial photosynthetic systems. *Acc. Chem. Res.* **2009**, *42* (12), 1910−1921.

(6) Sahoo, H. Förster resonance energy transfer − A spectroscopic nanoruler: Principle and applications. *J. Photochem. Photobiol., C* **2011**, *12* (1), 20−30.

(7) Furukawa, H.; Cordova, K. E.; O'Keeffe, M.; Yaghi, O. M. The chemistry and applications of metal-organic frameworks. *Science* **2013**, *341* (6149), 1230444.

(8) Hu, Z.; Deibert, B. J.; Li, J. Luminescent metal-organic frameworks for chemical sensing and explosive detection. *Chem. Soc. Rev.* **2014**, *43* (16), 5815−5840.

(9) Zhang, T.; Lin, W. Metal-organic frameworks for artificial photosynthesis and photocatalysis. *Chem. Soc. Rev.* **2014**, *43* (16), 5982−5993.

(10) So, M. C.; Wiederrecht, G. P.; Mondloch, J. E.; Hupp, J. T.; Farha, O. K. Metal-organic framework materials for light-harvesting and energy transfer. *Chem. Commun.* **2015**, *51* (17), 3501−3510.

(11) Xiao, J. D.; Jiang, H. L. Metal-Organic Frameworks for Photocatalysis and Photothermal Catalysis. *Acc. Chem. Res.* **2019**, *52* (2), 356−366.

(12) Rice, A. M.; Martin, C. R.; Galitskiy, V. A.; Berseneva, A. A.; Leith, G. A.; Shustova, N. B. Photophysics Modulation in Photoswitchable Metal-Organic Frameworks. *Chem. Rev.* **2020**, *120* (16), 8790−8813.

(13) Cao, W.; Tang, Y.; Cui, Y.; Qian, G. Energy Transfer in Metal−Organic Frameworks and Its Applications. *Small Struct.* **2020**, *1* (3), 2000019.

(14) Wang, Z.; Wang, C. Excited State Energy Transfer in Metal-Organic Frameworks. *Adv. Mater.* **2021**, 2005819.

(15) Lu, W.; Wei, Z.; Gu, Z. Y.; Liu, T. F.; Park, J.; Park, J.; Tian, J.; Zhang, M.; Zhang, Q.; Gentle Iii, T.; Bosch, M.; Zhou, H. C. Tuning the structure and function of metal-organic frameworks via linker design. *Chem. Soc. Rev.* **2014**, *43* (16), 5561−5593.

(16) Cao, L.; Lin, Z.; Shi, W.; Wang, Z.; Zhang, C.; Hu, X.; Wang, C.; Lin, W. Exciton Migration and Amplified Quenching on Two-Dimensional Metal-Organic Layers. *J. Am. Chem. Soc.* **2017**, *139* (20), 7020−7029.

(17) Zhu, J.; Maza, W. A.; Morris, A. J. Light-harvesting and energy transfer in ruthenium(II)-polypyridyl doped zirconium(IV) metal-organic frameworks: A look toward solar cell applications. *J. Photochem. Photobiol., A* **2017**, *344*, 64−77.

(18) Spoerke, E. D.; Small, L. J.; Foster, M. E.; Wheeler, J.; Ullman, A. M.; Stavila, V.; Rodriguez, M.; Allendorf, M. D. MOF-Sensitized Solar Cells Enabled by a Pillared Porphyrin Framework. *J. Phys. Chem. C* **2017**, *121* (9), 4816−4824.

(19) Maza, W. A.; Padilla, R.; Morris, A. J. Concentration Dependent Dimensionality of Resonance Energy Transfer in a Postsynthetically Doped Morphologically Homologous Analogue of UiO-67 MOF with a Ruthenium(II) Polypyridyl Complex. *J. Am. Chem. Soc.* **2015**, *137* (25), 8161−8168.

(20) Deria, P.; Yu, J.; Smith, T.; Balaraman, R. P. Ground-State versus Excited-State Interchromophoric Interaction: Topology Dependent Excimer Contribution in Metal-Organic Framework Photophysics. *J. Am. Chem. Soc.* **2017**, *139* (16), 5973−5983.
(21) Yu, J.; Anderson, R.; Li, X.; Xu, W.; Goswami, S.; Rajasree, S. S.; Maindan, K.; Gomez-Gualdron, D. A.; Deria, P. Improving Energy Transfer within Metal-Organic Frameworks by Aligning Linker Transition Dipoles along the Framework Axis. *J. Am. Chem. Soc.* **2020**, *142* (25), 11192−11202.
(22) Haldar, R.; Heinke, L.; Woll, C. Advanced Photoresponsive Materials Using the Metal-Organic Framework Approach. *Adv. Mater.* **2020**, *32* (20), 1905227.
(23) Goswami, S.; Yu, J.; Patwardhan, S.; Deria, P.; Hupp, J. T. Light-Harvesting "Antenna" Behavior in NU-1000. *ACS Energy Lett.* **2021**, *6* (3), 848−853.
(24) Lee, C. Y.; Farha, O. K.; Hong, B. J.; Sarjeant, A. A.; Nguyen, S. T.; Hupp, J. T. Light-harvesting metal-organic frameworks (MOFs): efficient strut-to-strut energy transfer in bodipy and porphyrin-based MOFs. *J. Am. Chem. Soc.* **2011**, *133* (40), 15858−15861.
(25) So, M. C.; Jin, S.; Son, H. J.; Wiederrecht, G. P.; Farha, O. K.; Hupp, J. T. Layer-by-layer fabrication of oriented porous thin films based on porphyrin-containing metal-organic frameworks. *J. Am. Chem. Soc.* **2013**, *135* (42), 15698−15701.
(26) Son, H. J.; Jin, S.; Patwardhan, S.; Wezenberg, S. J.; Jeong, N. C.; So, M.; Wilmer, C. E.; Sarjeant, A. A.; Schatz, G. C.; Snurr, R. Q.; Farha, O. K.; Wiederrecht, G. P.; Hupp, J. T. Light-harvesting and ultrafast energy migration in porphyrin-based metal-organic frameworks. *J. Am. Chem. Soc.* **2013**, *135* (2), 862−869.
(27) Williams, D. E.; Rietman, J. A.; Maier, J. M.; Tan, R.; Greytak, A. B.; Smith, M. D.; Krause, J. A.; Shustova, N. B. Energy transfer on demand: photoswitch-directed behavior of metal-porphyrin frameworks. *J. Am. Chem. Soc.* **2014**, *136* (34), 11886−11889.
(28) Park, J.; Feng, D.; Yuan, S.; Zhou, H. C. Photochromic metal-organic frameworks: reversible control of singlet oxygen generation. *Angew. Chem., Int. Ed.* **2015**, *54* (2), 430−435.
(29) Dolgopolova, E. A.; Williams, D. E.; Greytak, A. B.; Rice, A. M.; Smith, M. D.; Krause, J. A.; Shustova, N. B. A Bio-inspired Approach for Chromophore Communication: Ligand-to-Ligand and Host-to-Guest Energy Transfer in Hybrid Crystalline Scaffolds. *Angew. Chem., Int. Ed.* **2015**, *54* (46), 13639−13643.
(30) Goswami, S.; Chen, M.; Wasielewski, M. R.; Farha, O. K.; Hupp, J. T. Boosting Transport Distances for Molecular Excitons within Photoexcited Metal-Organic Framework Films. *ACS Appl. Mater. Interfaces* **2018**, *10* (40), 34409−34417.
(31) Roy, I.; Goswami, S.; Young, R. M.; Schlesinger, I.; Mian, M. R.; Enciso, A. E.; Zhang, X.; Hornick, J. E.; Farha, O. K.; Wasielewski, M. R.; Hupp, J. T.; Stoddart, J. F. Photon Upconversion in a Glowing Metal-Organic Framework. *J. Am. Chem. Soc.* **2021**, *143* (13), 5053−5059.
(32) Park, J.; Jiang, Q.; Feng, D.; Zhou, H. C. Controlled Generation of Singlet Oxygen in Living Cells with Tunable Ratios of the Photochromic Switch in Metal-Organic Frameworks. *Angew. Chem., Int. Ed.* **2016**, *55* (25), 7188−7193.
(33) Park, K. C.; Seo, C.; Gupta, G.; Kim, J.; Lee, C. Y. Efficient Energy Transfer (EnT) in Pyrene- and Porphyrin-Based Mixed-Ligand Metal-Organic Frameworks. *ACS Appl. Mater. Interfaces* **2017**, *9* (44), 38670−38677.
(34) Park, J.; Xu, M.; Li, F.; Zhou, H. C. 3D Long-Range Triplet Migration in a Water-Stable Metal-Organic Framework for Upconversion-Based Ultralow-Power in Vivo Imaging. *J. Am. Chem. Soc.* **2018**, *140* (16), 5493−5499.
(35) Kim, M.; Oh, J. S.; Kim, B. H.; Kim, A. Y.; Park, K. C.; Mun, J.; Gupta, G.; Lee, C. Y. Enhanced Photocatalytic Performance of Nanosized Mixed-Ligand Metal−Organic Frameworks through Sequential Energy and Electron Transfer Process. *Inorg. Chem.* **2020**, *59* (17), 12947−12953.
(36) Chakraborty, A.; Ilic, S.; Cai, M.; Gibbons, B. J.; Yang, X.; Slamowitz, C. C.; Morris, A. J. Role of Spin-Orbit Coupling in Long Range Energy Transfer in Metal-Organic Frameworks. *J. Am. Chem. Soc.* **2020**, *142*, 20434−20443.
(37) Jia, J.; Gutierrez-Arzaluz, L.; Shekhah, O.; Alsadun, N.; Czaban-Jozwiak, J.; Zhou, S.; Bakr, O. M.; Mohammed, O. F.; Eddaoudi, M. Access to Highly Efficient Energy Transfer in Metal-Organic Frameworks via Mixed Linkers Approach. *J. Am. Chem. Soc.* **2020**, *142* (19), 8580−8584.
(38) Gutierrez-Arzaluz, L.; Jia, J.; Gu, C.; Czaban-Jozwiak, J.; Yin, J.; Shekhah, O.; Bakr, O. M.; Eddaoudi, M.; Mohammed, O. F. Directional Exciton Migration in Benzoimidazole-Based Metal-Organic Frameworks. *J. Phys. Chem. Lett.* **2021**, *12* (20), 4917−4927.
(39) Liu, X. Y.; Ren, D.; Xia, H. L.; Zhou, K.; Wu, S.; Wang, X.; Li, J. Tuning and Directing Energy Transfer in the Whole Visible Spectrum through Linker Installation. *Angew. Chem., Int. Ed.* **2021**, *60*, 25048−25054.
(40) Zhang, X.; Frey, B. L.; Chen, Y. S.; Zhang, J. Topology-guided stepwise insertion of three secondary linkers in zirconium metal-organic frameworks. *J. Am. Chem. Soc.* **2018**, *140* (24), 7710−7715.
(41) Koh, K.; Wong-Foy, A. G.; Matzger, A. J. A crystalline mesoporous coordination copolymer with high microporosity. *Angew. Chem., Int. Ed.* **2008**, *47* (4), 677−680.
(42) Furukawa, H.; Ko, N.; Go, Y. B.; Aratani, N.; Choi, S. B.; Choi, E.; Yazaydin, A. O.; Snurr, R. Q.; O'Keeffe, M.; Kim, J.; Yaghi, O. M. Ultrahigh porosity in metal-organic frameworks. *Science* **2010**, *329* (5990), 424−428.
(43) Liu, L.; Konstas, K.; Hill, M. R.; Telfer, S. G. Programmed pore architectures in modular quaternary metal-organic frameworks. *J. Am. Chem. Soc.* **2013**, *135* (47), 17731−17734.
(44) Zhao, X.; Bu, X.; Zhai, Q. G.; Tran, H.; Feng, P. Pore space partition by symmetry-matching regulated ligand insertion and dramatic tuning on carbon dioxide uptake. *J. Am. Chem. Soc.* **2015**, *137* (4), 1396−1399.
(45) Liang, C. C.; Shi, Z. L.; He, C. T.; Tan, J.; Zhou, H. D.; Zhou, H. L.; Lee, Y.; Zhang, Y. B. Engineering of Pore Geometry for Ultrahigh Capacity Methane Storage in Mesoporous Metal-Organic Frameworks. *J. Am. Chem. Soc.* **2017**, *139* (38), 13300−13303.
(46) Yuan, S.; Qin, J. S.; Zou, L.; Chen, Y. P.; Wang, X.; Zhang, Q.; Zhou, H. C. Thermodynamically Guided Synthesis of Mixed-Linker Zr-MOFs with Enhanced Tunability. *J. Am. Chem. Soc.* **2016**, *138* (20), 6636−6642.
(47) Zhang, M.; Chen, Y. P.; Bosch, M.; Gentle, T., 3rd; Wang, K.; Feng, D.; Wang, Z. U.; Zhou, H. C. Symmetry-guided synthesis of highly porous metal-organic frameworks with fluorite topology. *Angew. Chem., Int. Ed.* **2014**, *53* (3), 815−818.
(48) Senthilkumar, K.; Kondratowicz, M.; Lis, T.; Chmielewski, P. J.; Cybinska, J.; Zafra, J. L.; Casado, J.; Vives, T.; Crassous, J.; Favereau, L.; Stepien, M. Lemniscular [16]Cycloparaphenylene: A Radially Conjugated Figure-Eight Aromatic Molecule. *J. Am. Chem. Soc.* **2019**, *141* (18), 7421−7427.
(49) Yuan, Y.; Huang, H.; Chen, L.; Chen, Y. *N,N′*-Bicarbazole: A Versatile Building Block toward the Construction of Conjugated Porous Polymers for CO_2 Capture and Dyes Adsorption. *Macromolecules* **2017**, *50* (13), 4993−5003.
(50) Boyer, G.; Claramunt, R. M.; Elguero, J.; Fathalla, M.; Foces-Foces, C.; Jaime, C.; Llamas-Saiz, A. L. Synthesis and structure of new hosts related to 9,9′-bianthryl. *J. Chem. Soc., Perkin Trans. 2* **1993**, No. 4, 757−766.
(51) Zhou, D.; Zhang, B.; Yu, Z.; Liao, Q.; Fu, H. tert-Butyl-substituted bicarbazole as a bipolar host material for efficient green and yellow PhOLEDs. *New J. Chem.* **2020**, *44* (25), 10472−10478.
(52) Rocquin, O.; Chevrot, C. Characterization and properties of the charge transfer complex of carbazole derivatives. *Synth. Met.* **1997**, *89* (2), 119−123.
(53) Liu, X. Y.; Zhang, Y. L.; Fei, X.; Liao, L. S.; Fan, J. 9,9′-Bicarbazole: New Molecular Skeleton for Organic Light-Emitting Diodes. *Chem. - Eur. J.* **2019**, *25* (17), 4501−4508.
(54) El-Mahdy, A. F. M.; Lai, M.-Y.; Kuo, S.-W. A highly fluorescent covalent organic framework as a hydrogen chloride sensor: roles of

https://doi.org/10.1021/jacs.1c10291
J. Am. Chem. Soc. XXXX, XXX, XXX−XXX

Schiff base bonding and π-stacking. *J. Mater. Chem. C* **2020**, *8* (28), 9520−9528.
(55) Deria, P.; Mondloch, J. E.; Tylianakis, E.; Ghosh, P.; Bury, W.; Snurr, R. Q.; Hupp, J. T.; Farha, O. K. Perfluoroalkane functionalization of NU-1000 via solvent-assisted ligand incorporation: synthesis and CO_2 adsorption studies. *J. Am. Chem. Soc.* **2013**, *135* (45), 16801−16804.
(56) Blatov, V. A.; Shevchenko, A. P.; Serezhkin, V. N. TOPOS3.2: a new version of the program package for multipurpose crystal-chemical analysis. *J. Appl. Crystallogr.* **2000**, *33* (4), 1193−1193.
(57) Zhang, Y. B.; Furukawa, H.; Ko, N.; Nie, W.; Park, H. J.; Okajima, S.; Cordova, K. E.; Deng, H.; Kim, J.; Yaghi, O. M. Introduction of functionality, selection of topology, and enhancement of gas adsorption in multivariate metal-organic framework-177. *J. Am. Chem. Soc.* **2015**, *137* (7), 2641−2650.
(58) Liu, Q.; Cong, H.; Deng, H. Deciphering the Spatial Arrangement of Metals and Correla-tion to Reactivity in Multivariate Metal-Organic Frameworks. *J. Am. Chem. Soc.* **2016**, *138*, 13822−13825.
(59) Deng, H.; Doonan, C. J.; Furukawa, H.; Ferreira, R. B.; Towne, J.; Knobler, C. B.; Wang, B.; Yaghi, O. M. Multiple functional groups of varying ratios in metal-organic frameworks. *Science* **2010**, *327* (5967), 846−850.
(60) Feng, D.; Gu, Z. Y.; Li, J. R.; Jiang, H. L.; Wei, Z.; Zhou, H. C. Zirconium-metalloporphyrin PCN-222: mesoporous metal-organic frameworks with ultrahigh stability as biomimetic catalysts. *Angew. Chem., Int. Ed.* **2012**, *51* (41), 10307−10310.
(61) Feng, D.; Chung, W. C.; Wei, Z.; Gu, Z. Y.; Jiang, H. L.; Chen, Y. P.; Darensbourg, D. J.; Zhou, H. C. Construction of ultrastable porphyrin Zr metal-organic frameworks through linker elimination. *J. Am. Chem. Soc.* **2013**, *135* (45), 17105−17110.
(62) Jin, S.; Son, H. J.; Farha, O. K.; Wiederrecht, G. P.; Hupp, J. T. Energy transfer from quantum dots to metal-organic frameworks for enhanced light harvesting. *J. Am. Chem. Soc.* **2013**, *135* (3), 955−958.
(63) Kent, C. A.; Mehl, B. P.; Ma, L.; Papanikolas, J. M.; Meyer, T. J.; Lin, W. Energy transfer dynamics in metal-organic frameworks. *J. Am. Chem. Soc.* **2010**, *132* (37), 12767−12769.
(64) Dolgopolova, E. A.; Rice, A. M.; Martin, C. R.; Shustova, N. B. Photochemistry and photophysics of MOFs: steps towards MOF-based sensing enhancements. *Chem. Soc. Rev.* **2018**, *47* (13), 4710−4728.

https://doi.org/10.1021/jacs.1c10291
J. Am. Chem. Soc. XXXX, XXX, XXX−XXX